Folding Kinetics of Phage 434 Cro Protein†

D. V. Laurents,‡,§ S. Corrales,|| M. Elías-Arnanz,⊥ P. Sevilla,|| M. Rico,‡ and S. Padmanabhan*,⊥

Instituto de Estructura de la Materia, Consejo Superior de Investigaciones Científicas, Serrano 119, 28006 Madrid, Spain, Departamento de Genética y Microbiología, Facultad de Biología, Universidad de Murcia, 30071 Murcia, Spain, and Departmento de Física Química II, Facultad de Farmacia, Universidad Complutense, 28040 Madrid, Spain

Received June 19, 2000; Revised Manuscript Received September 1, 2000

ABSTRACT: Folding kinetics for phage 434 Cro protein are examined and compared with those reported for λ_{6-85}, the N-terminal domain of the repressor of phage λ. The two proteins have similar all-helical structures consisting of five helices but different stabilities. In contrast to λ_{6-85}, sharp and distinct aromatic ^{1}H NMR signals without exchange broadening characterize the native and urea-denatured 434 Cro forms at equilibrium at 20 °C, indicating slow interconversion on the NMR time scale. Stopped-flow fluorescence data using the single 434 Cro tryptophan indicate strongly urea-dependent refolding rates and smaller urea dependencies of the unfolding rates, suggesting a native-like transition state ensemble. Refolding rates are slower and unfolding rates considerably faster at pH 4 than at pH 6. This accounts for the lower stability of 434 Cro at pH 4 and suggests the existence of pH-dependent, possibly salt bridge interactions that are more stabilizing at pH 6. At <2 M urea, decreased folding amplitudes and nonlinear urea dependencies that are apparent at pH 6 indicate deviation from two-state behavior and suggest the formation of an early folding intermediate. The folding behavior of 434 Cro and why it folds 2 orders of magnitude slower than λ_{6-85} are rationalized in terms of the lower intrinsic helix stabilities and putative charge interactions in 434 Cro.

Levinthal argued in 1968 that proteins cannot fold by a random sampling of conformations because this would require an enormously long search time (*1*). The formation of folding intermediates can serve to reduce the conformational space to be sampled and to channel folding toward a productive pathway, and productive folding intermediates have indeed been observed for various proteins (*2*, *3*). More recently, this view of intermediates being essential midwives in the folding process has been challenged by the finding that some intermediates contain non-native interactions and retard folding, thus behaving more like kinetic traps (*4*−*11*). The idea that intermediates serve as necessary stepping stones for protein folding is further disputed by the finding that many small proteins (around 80 or fewer residues) fold extremely rapidly (in milliseconds or less) without populated intermediates (*12* and references therein). Computer simulations that model polypeptide conformational changes also suggested that folding could follow multiple channels (like water flowing down a rough funnel) and that defined intermediates are not essential to overcoming the Levinthal paradox (*13*, *14*). The recent emerging view thus emphasizes multiple folding pathways with ensembles as opposed to unique intermediates and transition states (*13*, *14*).

The rapid folding of small proteins without observable intermediates could be a consequence of their small size, and their lack of cis prolines or tightly bound ligands. Perhaps these proteins fold rapidly because they are too small to give rise to any stable intermediates, unlike in the case of larger proteins. Or it could be that the intermediates they form are too transient to characterize. Studies of short protein fragments show that marginally, stable structures such as α-helices, β-turns, or β-hairpins can form extremely rapidly and that their structures and interactions are conserved in the native protein, suggesting a means of avoiding an exhaustive sampling of conformational space (*3*). These observations and the recent view of several independent folding pathways were melded into a diffusion−collision model in which folding begins with the transient formation of a number of different local units of structure or nuclei, which then associate by diffusion and collision via distinct pathways that converge to form the folded protein (*15*). This model was used to describe the experimentally observed rapid folding behavior of the monomeric, helical, 80-residue N-terminal domain of the λ repressor, λ_{6-85},[1] and its variants, where it was concluded that local helix stabilities are important in determining folding rates (*16*). Moreover, like in many helical proteins, the majority of interresidue contacts in λ_{6-85} are local (between residues close in sequence) as opposed to long-range, and this low "contact order" has been correlated with its rapid folding behavior (*17*).

† Supported by Grants PB93-0189 (DGICYT- Spain) and B104-CT97-2086 (EU) to M.R. D.V.L. is a postdoctoral fellow of the Leukemia and Lymphoma Society of America.

* Corresponding author. Telephone: +34 (91) 561-9400. Fax: +34 (91) 564-2431. E-mail: padhu@um.es.

‡ Consejo Superior de Investigaciones Científicas.

§ Present address: Universidad Internacional SEK, c/ Cardenal Zúñiga s/n, 40003 Segovia, Spain.

|| Universidad Complutense.

⊥ Universidad de Murcia.

[1] Abbreviations: CD, circular dichroism; DTT, dithiothreitol; λ_{6-85}, N-terminal monomeric domain of the λ repressor; NMR, nuclear magnetic resonance; TOCSY, total correlation spectroscopy; TSP, [2,2,3,3-$^2H_4$]trimethylsilyl.

10.1021/bi001388d CCC: $19.00
Published on Web 10/21/2000

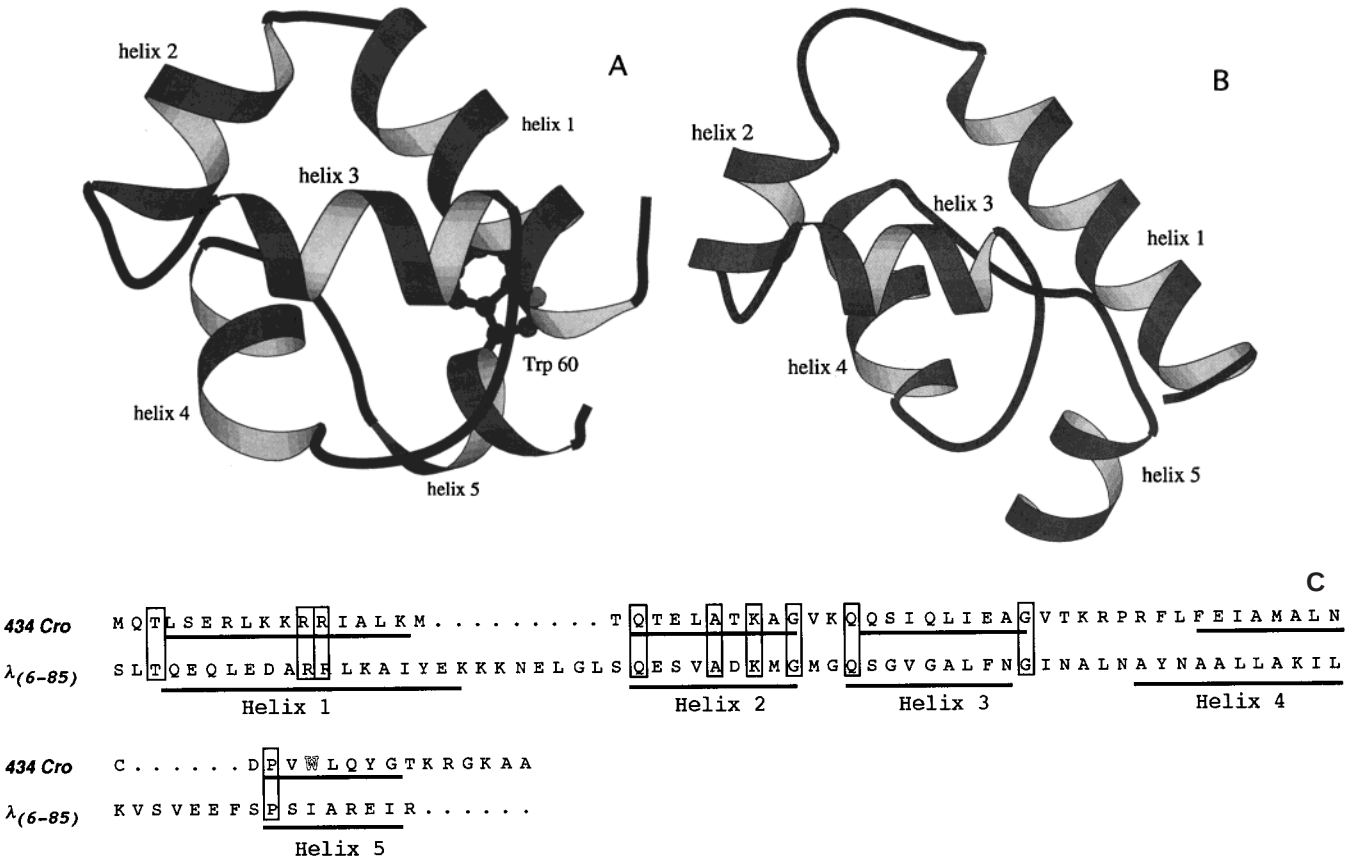

FIGURE 1: Structures of 434 Cro (A) and λ_{6-85} (B) generated using Molscript (*68*) and their sequences (C). Helix numbers and the single Trp in 434 Cro are indicated, and helical residues are underlined in the sequences. Sequence positions with identical residues are in blocks.

An experimental approach to studying folding mechanisms is examining how specific mutations in a protein affect its stability and kinetics of folding, an approach commonly termed the "protein engineering" method (*18*, *19*). This has been applied for various proteins, including λ_{6-85} (*20*). Alternatively, the folding mechanisms of structurally similar proteins can be compared (*21*−*25*). The 71-residue, helix−turn−helix DNA-binding protein of phage 434 is composed of five helices as in λ_{6-85}, and their coincident backbone conformations would be expected to result in very similar contact orders (Figure 1; *26*−*28*). The two proteins share 10 conserved residues, almost all of which are in the first three helices (Figure 1). Both proteins exhibit two-state equilibrium folding behavior, with 434 Cro being less stable (*28*−*30*). Using synthetic peptide fragments, intrinsic folding propensities have been experimentally evaluated for all the helices in 434 Cro (*31*) and for helix 1 of λ_{6-85} (*32*). The kinetics of folding though examined for λ_{6-85} (*16*, *20*) are, to our knowledge, as yet unavailable for 434 Cro. We therefore set out to measure the folding kinetics for 434 Cro to compare its behavior with that of λ_{6-85}, and to gain further insight into the links between structure, stability, and folding mechanisms for small, all-helical proteins.

EXPERIMENTAL PROCEDURES

Materials. 434 Cro was overexpressed using the T7 promoter-based pET11b construct and purified as described previously and the purity checked in a 15% SDS−PAGE gel with Coomassie blue staining and by analytical reverse-phase HPLC (*28*, *29*). Protein concentrations were based on the absorbance at 280 nm using extinction coefficients (ϵ_{280}) of 6935 and 6370 cm^{-1} M^{-1}, respectively, for denatured and native 434 Cro as reported previously (*29*). Ultrapure urea was from ICN Biomedicals (Aurora, OH). Other chemicals were from Sigma (St. Louis, MO) or Merck (Darmstadt, Germany). The salt and buffer concentrations were 100 mM KCl and 25 mM KH_2PO_4 for solutions at pH 6 (pH 6 buffer) or 100 mM KCl and 25 mM potassium acetate for those at pH 4 (pH buffer). DTT (1 mM) or β-mercaptoethanol was included to prevent oxidation of the single cysteine residue in 434 Cro. Urea stocks at the appropriate salt and buffer concentrations were prepared afresh as described by Pace and Scholtz (*33*) and used promptly to minimize possible urea breakdown products. Experiments were carried out at 20 °C unless stated otherwise.

CD and NMR Measurements. Circular dichroism (CD) experiments were carried out in a Jasco J720 spectropolarimeter equipped with a computer-controlled Neslab water bath unit for temperature control. Equilibrium urea-induced folding−unfolding transitions were examined by far-UV CD and the data analyzed using procedures described previously (*28*, *29*). Manual mixing kinetic experiments were monitored by far-UV CD using a 1 cm path length cell. Refolding jumps were made by diluting (1:10) the protein unfolded in 7 M urea into pH 6 buffer to a final urea concentration of 0.7 M (where the native state is fully populated) or close to the transition midpoint where folded and unfolded molecules are nearly equally populated and where folding kinetics are generally slowest. The final protein concentration was 25

μM. After manual mixing, the evolution with time of the CD signal at 222 nm, which is proportional to helicity, was followed. The experimental dead time was about 30 s.

One-dimensional ^{1}H NMR spectra (16 kb, 3 s relaxation recycle delay, 64 scans) were recorded on a Bruker AMX-600 spectrometer. 434 Cro at initial concentrations of 0.1−0.5 mM in D_2O was titrated with deuterated urea solutions at 20 °C in pH 6 buffer. Two-dimensional ^{1}H TOCSY (*34*) of 434 Cro in 4 M urea solutions where both native and denatured forms of the protein are present was used to assign the aromatic ring protons in each form relative to TSP, used as the internal chemical shift standard, and checked with those assigned previously for the native protein and its fragments in 7 M urea (*28*, *31*).

Stopped-Flow Fluorescence. Stopped-flow kinetics were determined on a Biologic (Grenoble, France) MSP-4 stopped-flow device with four syringes coupled to a fluorescence apparatus using a 1.5 mm path length FC-15 cuvette. The protein and buffers in the syringes, the mixing block, and the detection chamber were thermostated by a circulating temperature-controlled water bath. The excitation wavelength that was used was 295 nm, and the total fluorescence emission after passing a 325 nm cutoff filter to eliminate the Raman component was recorded. Protein (25 or 40 μL, native for unfolding experiments and urea-denatured for refolding experiments) was mixed with varying ratios of buffer and a concentrated urea solution to obtain the desired final urea concentration. The final protein concentration was around 3.2 μM. Usually three mixing shots were recorded for each final urea concentration. The estimated dead time was 6.2 ms. In one set of experiments, the apparent folding rate was measured in 1.5 M urea over a range of different temperatures. Exponential fits to the folding and unfolding traces were determined using the supplied Biologic software or Kaleidagraph (Synergy Software, PCS Inc.) as follows

$$I(t) = I_\infty + (I_0 - I_\infty)e^{-k_{obs}t} \quad (1)$$

where $I(t)$, I_0, and I_∞ are the fluoresence signal at time t and the initial and final values, respectively, $I_0 - I_\infty$ is the amplitude, and k_{obs} is the observed rate. For a two-state, native unfolded (N ⇔ U) transition, k_{obs} equals the sum of the rate constants for unfolding (k_u) and folding (k_f), whose dependencies on urea concentration, [Ur], are modeled as follows (*35*):

$$\ln k_u = \ln k_u^0 + m_u[\mathrm{Ur}] \quad (2a)$$

$$\ln k_f = \ln k_f^0 + m_f[\mathrm{Ur}] \quad (2b)$$

$$\ln k_{obs} = \ln(k_u + k_f) = \ln(k_u^0 e^{m_u[\mathrm{Ur}]} + k_f^0 e^{m_f[\mathrm{Ur}]}) \quad (2c)$$

The ln k_{obs} versus [Ur] data fit to eq 2c yield k_u^0 and k_f^0, the rate constants for [Ur] = 0, and the corresponding urea dependence slopes m_u and m_f. These kinetic parameters at a given temperature (T) are related to the equilibrium parameters K_u, $\Delta G_u(T,[\mathrm{Ur}])$, m_{eq}, and C_m which are the equilibrium constant, the unfolding free energy, the equilibrium m value, and the urea concentration at the transition midpoint, respectively, as follows:

$$\Delta G_u(T,[\mathrm{Ur}]) = \Delta G_u(T,0) - m_{eq}[\mathrm{Ur}] = -RT \ln K_u = -RT \ln(k_u/k_f) \quad (3a)$$

$$m_{eq} = RT(m_u - m_f) \quad (3b)$$

$$C_m = \Delta G_u(T,0)/m_{eq} = \ln(k_u^0/k_f^0)/(m_f - m_u) \quad (3c)$$

The position of the transition state ensemble between the denatured and native states can be gauged in terms of the following parameter:

$$\alpha = m_u/(m_u - m_f) \quad (4)$$

Since for a given transition the m value is directly related to the accompanying change in the extent of solvent exposure (*35*), α is a measure of the solvent exposure of the transition state ensemble relative to the denatured and native states; α is closer to 0 for a native-like transition state ensemble where the change in the extent of solvent exposure is low and is closer to 1 when the transition state is more solvent-exposed like in the denatured state.

Kinetic Simulations. Simulation of the pH 6, 20 °C folding data was carried out using HopKINSIM (version 1.3). The simulations were carried out for 2 s, integrating an 8 b point every 10 ms. 434 Cro is assumed to fold via an on-pathway intermediate, I, that is populated at low urea concentrations, has a native-like fluorescence signal, and is in rapid equilibrium with the unfolded state U. The height of the transition state ensemble barrier (‡) between I and the native state N was calculated using the Eyring equation (*36*) and the observed reaction rate. The fractional m values of I and ‡ were varied until a good match with the experimental data was obtained. The midpoint of the U ⇔ I transition was estimated by fitting the dead-time amplitude versus [Ur] to the two-state model.

RESULTS

Equilibrium Folding of 434 Cro. 434 Cro folding at equilibrium conforms to a two-state model as inferred from chemical and thermal denaturation studies as well as from calorimetry (*28*, *29*). Calorimetric data indicated that ΔG_u for 434 Cro decreases with pH and that unfolding appears to occur with a net uptake of about one proton at pH 4 and essentially zero by pH 5 (*29*). Therefore, the folding kinetics of 434 Cro were examined in this study at pH 6 as well as at pH 4 (see below). Figure 2 shows equilibrium urea-induced folding transitions at 20 °C and pH 4 obtained in this study and those at pH 6 reported previously (*29*). The corresponding parameters from a two-state analysis of the folding equilibrium are listed in Table 1. m_{eq} at pH 4 significantly exceeds that at pH 6. Increases in m_{eq} with decreasing pH have been observed with a number of other proteins, and are generally attributed to an increased level of solvent exposure of the unfolded state (*37*), although exceptions to this have also been reported (*38*, *39*). ΔG_u at pH 6 is greater than at pH 4 which is consistent with calorimetric data. However, ΔG_u from urea denaturation at pH 4, unlike that at pH 6, is found to be significantly greater than the value expected from calorimetric data at the same pH, where ΔG_u(25 °C) = 1.55 ± 0.1 kcal/mol (*29*). The discrepancy

Table 1: Equilibrium and Kinetic Parameters for 434 Cro Urea-Induced Folding Transitions[a]

	pH 6.0		pH 4.0	
	equilibrium[b]	kinetics	equilibrium	kinetics
m_{eq} (kcal mol^{-1} M^{-1})	1.01 ± 0.12	0.97 ± 0.10 (0.98 ± 0.07)*	1.28 ± 0.07	1.34 ± 0.04 (1.34 ± 0.06)*
C_m (M urea)	3.42 ± 0.09	3.43 ± 0.50 (3.46 ± 0.50)*	1.93 ± 0.05	1.29 ± 0.12 (1.33 ± 0.13)*
ΔG_u (kcal mol^{-1})	3.44 ± 0.47	3.34 ± 0.20 (3.39 ± 0.16)*	2.47 ± 0.19	1.73 ± 0.07 (1.78 ± 0.11)*

[a] At 20 °C with 100 mM KCl, 25 mM KH_2PO_4 (pH 6) or 25 mM CH_3COOK (pH 4), and 1 mM DTT. Equilibrium values are from far-UV CD data; kinetic data are from stopped-flow fluorescence analyzed using a two−state model as listed in Table 2. [b] From ref *29*. In parentheses with an asterisk are the values obtained by analyzing rates corrected for urea-dependent viscosity effects (see the text).

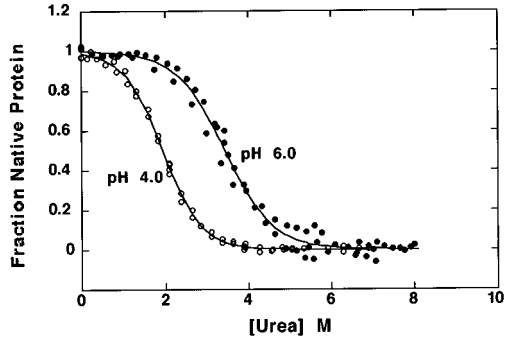

FIGURE 2: Urea-induced equilibrium folding transitions monitored by far-UV CD at 20 °C for 434 Cro at pH 4.0 (○) and 6.0 (●). Solution conditions included protein (~25 μM), 100 mM KCl, 1 mM DTT with 25 mM KH_2PO_4 (pH 6.0 buffer), or 25 mM CH_3-COOK (pH 4.0 buffer). Continuous curves are fits to the data analyzed using procedures described previously (*28*, *29*).

could be a consequence of uncertainties associated with the native baselines being insufficiently long for accurate analysis (*33*; Figure 2).

Folding−Unfolding Interconversions at Equilibrium from NMR. Interconversions between the folded and unfolded states at equilibrium can, in principle, be monitored using the behavior of the ^{1}H NMR chemical shifts of nonexchangeable, typically aromatic, resonances. Under conditions where both the folded and unfolded states are significantly populated, distinct resonances are observed for each state when they interconvert slowly on the NMR time scale. On the other hand, fast or intermediate exchange causes the NMR signals to coalesce into a single, broadened average peak whose line-shape analysis provides estimates for the interconversion rate. Urea-induced N ⇔ U transitions at ≤37 °C are fast on the NMR time scale for λ_{6-85} and many of its variants, and line-shape analysis of the aromatic exchange-broadened peaks yielded interconversion rates in the sub-millisecond (20−250 μs) time range (*16*, *20*). By contrast, distinct aromatic NMR peaks without any exchange broadening are observed for native and urea-unfolded 434 Cro at 20 °C and pH 6, indicating interconversions that are slow on the NMR time scale (Figure 3) (aromatic residues in 434 Cro and λ_{6-85} shown in Figure 1). Since only the folded and unfolded resonances are observed, intermediates are either absent or insignificantly populated, or they overlap with the native and/or unfolded signals under these equilibrium conditions. The chemical shift difference, $\Delta\delta$ (in hertz), provides a limit for this slow interconversion rate: $k \ll 2\pi\Delta\delta$ and time constant $\tau = 1/k$ (*40*). At urea concentrations close to C_m (Table 1), the maximum $\Delta\delta$ for the 434 Cro aromatic protons is 0.22 ppm (132 Hz) so that $k \ll 850$ s^{-1} ($\tau \gg 1.2$ ms). N ⇔ U interconversions can be sped up by increasing temperatures to near T_m in the thermal denaturation zone to obtain

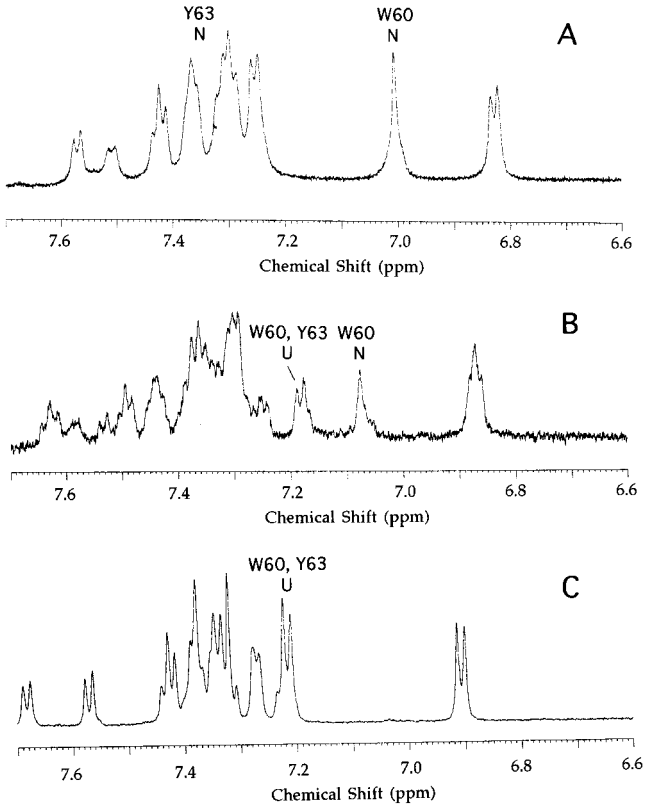

FIGURE 3: One-dimensional ^{1}H NMR spectra of 434 Cro in 0 M urea [native (A)] and 3.75 M urea [in the transition zone (B)] and unfolded in 6.5 M urea (C) at 20 °C in pH 6.0 buffer as described in the legend of Figure 2 but in 100% D_2O. The folded and unfolded resonances of Trp60 and Tyr63 are indicated.

exchange-broadened NMR signals amenable to line-shape analysis (*41*). This was not possible with 434 Cro because the aromatic resonances overlap considerably near T_m and the thermal transitions are not reversible at NMR protein concentrations (*28*, *29*).

Refolding and Unfolding Kinetics from Stopped-Flow Fluorescence. The experiments described above suggested that N ⇔ U interconversions occur with time constants well above 1 ms, and that intermediates are either absent or insignificantly populated under these equilibrium conditions. They do not, however, rule out the possibility that intermediates form transiently along the folding pathway. This can be detected only in time-resolved kinetic experiments. In manual mixing experiments, complete folding was achieved within the 30 s dead time even for final urea concentrations close to C_m where refolding is slowest (data not shown). Together with the NMR observations, this indicates that 434 Cro folds in the time range of milliseconds to a few seconds.

Stopped-flow measurements provide a detailed, time-resolved characterization of folding−unfolding kinetics, and

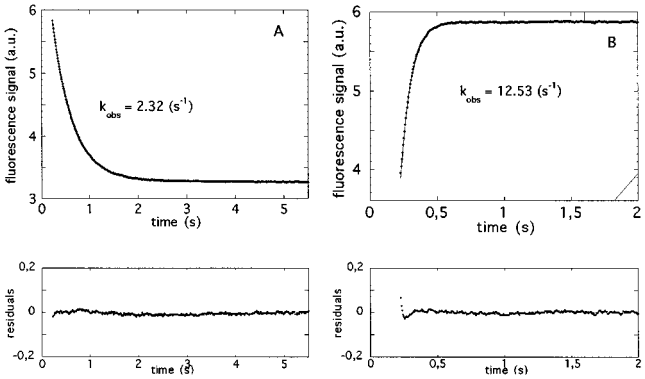

FIGURE 4: Typical fluorescence-detected stopped-flow kinetic traces for 434 Cro at pH 6.0 and 20 °C. (A) Native 434 Cro unfolding in 8.5 M urea. (B) Unfolded 434 Cro in 6 M urea refolding in a final urea concentration of 1.92 M. In both panels, the residuals after fitting to a single-exponential equation are shown at the bottom.

can detect intermediates that cannot be observed under equilibrium conditions. 434 Cro contains a single Trp residue whose emission maximum of around 348 nm in the native protein shifts to around 353 nm upon urea denaturation with a ~50% drop in intrinsic fluorescence intensity (*28*). This provides a sensitive optical probe for stopped-flow fluorescence measurements of folding kinetics. By contrast, the absence of Trp in λ_{6-85} necessitated a specifically engineered Trp variant (*42*). Figure 4 shows typical kinetic traces for refolding and unfolding which, in general, are well fit by single exponentials (eq 1). In some traces, a slow, minor refolding phase was observed and could possibly be attributed to proline isomerization (*43*). Native 434 Cro has two *trans* (*t*) Pro residues, P44 and P58 (Figure 1), which, under unfolding conditions, would equilibrate with the *cis* (*c*) form to produce a population distribution for the two Pro residues of about 85.0% P44*t*/P58*t*, 7.2% P44*t*/P58*c*, 7.3% P44*c*/P58*t*, and around 0.5% Pro44*c*/P58*c* (*44*). The slow refolding of the unfolded species with *cis* Pro could account for the occasionally observed minor slow phase, and is not considered further here.

Single-exponential fits of stopped-flow fluorescence data obtained at pH 4 or 6 and for various urea concentrations yield the rates and amplitudes shown in Figure 5. Unfolding rates for 434 Cro show small urea dependencies and are more rapid at pH 4 than at pH 6. Refolding rates at the two pH values are sensitive to urea concentration and are slower at pH 4. The straight lines in Figure 5 correspond to two-state model fits (eq 2) of ln *k* versus [Ur] data (chevron plots) with k_u^0, k_f^0, m_u, and m_f listed in Table 2. The two-state model fitting used all the data obtained at pH 4, but only data at >2 M urea and pH 6, those below 2 M urea being excluded because they deviate from the expected linearity. The implications of this deviation will be discussed subsequently. Table 2 includes the two-state kinetic parameters at 20 °C reported for the fast folding λ_{6-85} variant (λ_{6-85}*) in which a Trp was introduced to enable stopped-flow fluorescence studies (*42*). Table 2 also includes the parameters estimated by NMR line-shape analysis for wild-type λ_{6-85} at 25 °C (*45*). The two-state refolding rate extrapolated to zero urea, k_f^0, for 434 Cro is slower than for λ_{6-85}* or for wild-type λ_{6-85} by about 3 or 2 orders of magnitude, respectively. In contrast, the unfolding rate of 434 Cro in 0 M urea, k_u^0, differs from that reported for λ_{6-85} or its variant by ≤1 order of magnitude. As with λ_{6-85}, the two-state m_u and m_f values yield low α values (eq 4) of <0.2. This suggests that of the total surface area buried upon folding, more than three-quarters is inaccessible to solvent by the time the transition state ensemble is reached, indicating that the latter is native-like in terms of the extent of solvent exposure.

ΔG_u, m_{eq}, and C_m for 434 Cro based on its two-state kinetic parameters (eq 3) are not coincident with their equilibrium values (Table 1). This suggests deviation from two-state behavior. This is also manifested in the apparent downward curvature ("rollover") in the refolding limb accompanied by an amplitude decrease for urea concentrations of <1.5 M in the chevron plot for pH 6 (Figure 5A). There is no evidence for this being dependent on protein concentration and so on aggregation. At pH 4, such a rollover and amplitude loss in the refolding limb are either negligibly small or absent, but the unfolding limb appears to flatten out at the highest urea concentrations. Protein stability is low at pH 4, and the shorter folded baseline that results (Figure 2) may not be sufficiently long to detect any rollover and accompanying amplitude loss at this pH (*22*). The shorter folded baseline could also, as noted earlier, affect estimates for the corresponding equilibrium values and account, at least partly, for the difference between the kinetic and equilibrium ΔG_u and C_m values at pH 4.

Analysis of Rollover and Decreasing Amplitudes in Kinetic Data. Different phenomena can explain the observed curvature in chevron plots. The experimental evidence presently available in the literature indicates protein folding and unfolding kinetics are dependent on solvent viscosity effects, and k_{obs} values need to be corrected using the expression (*46*):

$$\ln k_{obs}(\text{corrected}) = \ln k_{obs} + \ln(\eta/\eta_0) \qquad (5)$$

Here η and η_0 are the viscosities in the presence and absence of urea (*47*). Figure 5 shows the effects of such a correction on the observed rates. The viscosity correction is negligible at low urea concentrations but is significant at the highest urea concentrations. This effectively increases the slope of the unfolding limb, m_u, and extrapolates to a slower k_u^0, and the resulting variations in the other kinetic parameters are indicated in Tables 1 and 2. The correction for urea-dependent viscosity effect results in a less discernible flattening out at higher urea concentrations for the pH 4 unfolding limb, but cannot explain the rollover observed at low urea concentrations and pH 6.

Rollover and the decreased folding amplitudes at low urea concentrations are classic evidence for the existence of metastable intermediate(s) that accumulate rapidly on refolding (*3*, *11*, *19*, *23*, *38*, *39*, *48*−*50*). In this case, the rollover and amplitude loss can be modeled by a three-state model as follows (*39*):

$$\mathrm{U} \underset{k_{IU}}{\overset{k_{UI}}{\rightleftharpoons}} \mathrm{I} \underset{k_{NI}}{\overset{k_{IN}}{\rightleftharpoons}} \mathrm{N} \qquad (6)$$

Here I, assumed to be on-pathway, corresponds to a dynamic ensemble of partially folded intermediates with native-like fluorescence properties and k_{UI}, k_{IU}, k_{IN}, and k_{IN} are rate constants. Assuming that the concentration of I at the start of folding can be approximately quantified by the amount of amplitude missing according to the two-state model and

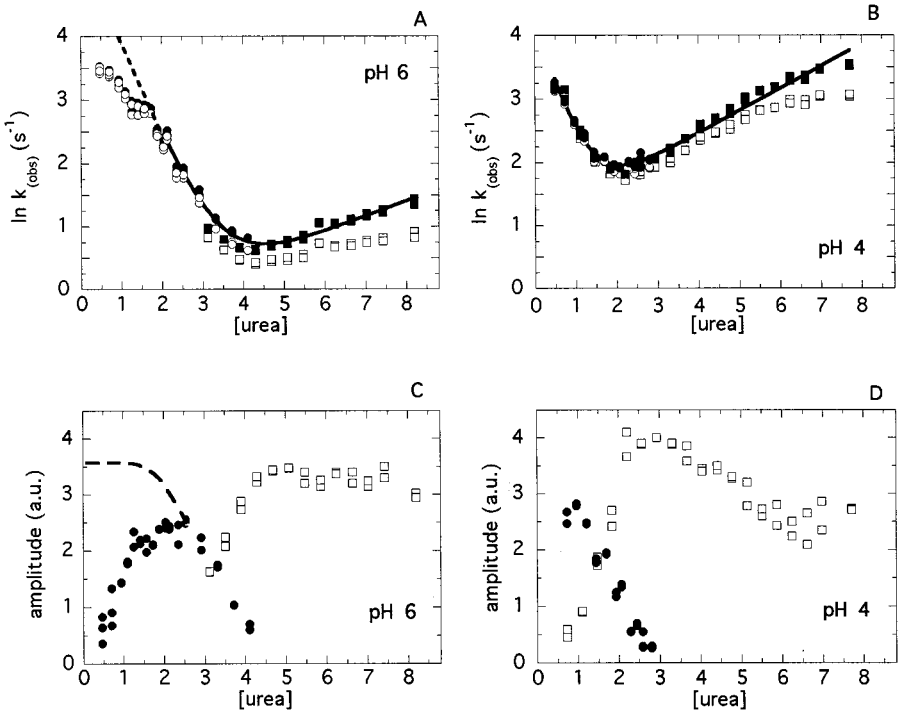

FIGURE 5: Folding and unfolding rates and amplitudes for 434 Cro taken from stopped-flow fluorescence measurements at 20 °C. The plot of ln k_{obs} vs [Ur] at pH 6 and 4 is shown in the top panels (A and B), while the corresponding amplitudes at various urea concentrations are shown in panels C and D in the bottom. Circles in all panels indicate refolding, and squares indicate unfolding. In panels A and B, the black symbols indicate k_{obs} corrected for urea-dependent viscosity effects and the straight lines are fits to a two-state model as described in the text. The dashed lines in panels A and C show the behavior expected for two-state folding. The black symbols in panels C and D indicate folding and the white symbols unfolding.

Table 2: Kinetic Parameters for 434 Cro and λ_{6-85} from Stopped-Flow Fluorescence Data at 20 °C Analyzed Using a Two-State Model

	434 Cro[a] at pH 6	434 Cro[a] at pH 4	λ_{6-85}*[b] at pH 8	λ_{6-85}[c] at pH 8
k_f^0 (s^{-1})	210 ± 50 (200 ± 40)*	61 ± 6 (62 ± 6)*	(61 ± 18) × 10^3	(11.1 ± 3) × 10^3
k_u^0 (s^{-1})	0.68 ± 0.11 (0.59 ± 0.10)*	3.14 ± 0.16 (2.92 ± 0.14)*	(3.6 ± 1.0)	(9.24 ± 2.8)
m_f (kcal mol^{-1} M^{-1})	−0.88 ± 0.06 (−0.83 ± 0.06)*	−1.18 ± 0.06 (−1.14 ± 0.06)*	−(0.81 ± 0.03)	-(0.81 ± 0.04)
m_u (kcal mol^{-1} M^{-1})	0.09 ± 0.02 (0.14 ± 0.01)*	0.16 ± 0.01 (0.20 ± 0.20)*	(0.20 ± 0.05)	(0.29 ± 0.04)
α	0.10 ± 0.20 (0.14 ± 0.10)*	0.12 ± 0.07 (0.15 ± 0.07)*	(0.20 ± 0.04)	(0.26 ± 0.04)

[a] With 100 mM KCl, 25 mM KH_2PO_4 (pH 6) or 25 mM CH_3COOK (pH 4), and 1 mM DTT. At pH 6, only data at >2 M urea were fit. [b] With 100 mM NaCl and 20 mM potassium phosphate for a G46A/G48A/Y22W variant (*42*). [c] From NMR line-shape analysis for the wild-type protein at 25 °C (*45*). The values obtained by analyzing rates corrected for urea-dependent viscosity effects (see the text) are shown in parentheses with an asterisk.

that I and U interconvert rapidly, we estimate that this interconversion occurs with an apparent C_m of 0.9 M urea for 434 Cro. Using this value and the three-state mechanism shown above, it was possible to simulate the observed folding kinetics at pH 6 and 20 °C in urea (Figure 6). According to the simulation, I has a stability of approximately −0.6 kcal mol^{-1} at 0 M urea and an *m* value of approximately 700 cal mol^{-1} M^{-1}. The latter result leads to the inference that the majority of nonpolar surface in I is buried, since m_{eq} at pH 6 is around 1000 cal mol^{-1} M^{-1}. Burial of Trp60 that produces the increase in fluorescence emission would then occur in the fast U ⇔ I step. The transition state ensemble would have an *m* value of approximately 800 cal mol^{-1} M^{-1} and has a high free energy (about 15 kcal mol^{-1}). Rather than in terms of intermediate formation, downward curvature in chevron plots has also been attributed to shifts in the position of the transition state ensemble with varying denaturant concentrations, but these appear to occur without any pronounced amplitude decline (*23*). Such an effect could thus explain in part the flattening out of the pH 4 unfolding limb in high urea, but not the rollover as well as amplitude loss observed with the pH 6 refolding limb at low urea concentrations.

Temperature Dependence of Observed Folding Rates. The refolding rates of 434 Cro in 1.5 M urea in pH 6 buffer at various temperatures between 17 and 40 °C are shown in Figure 7. The folding rate increases with temperature. As described by Chen et al. (*51*), the data were replotted as $\ln(k_f^{\ddagger})$ versus $1/T$ and fit to the equation

$$\ln(k_f^{\ddagger}) = \ln(k_f h/k_B T) = A + B(T_0/T) + C\ln(T_0/T) \qquad (7)$$

where k_B is Boltzmann's constant, *h* is Planck's constant, *T* is the absolute temperature, T_0 is a reference temperature, and *A*, *B*, and *C* are constants (as defined in ref *51*) and are evaluated by nonlinear regression. In particular, $C = \Delta C_p^{\ddagger}/R$, where $\Delta C_p^{\ddagger}$ is the activation heat capacity change and *R* is the gas constant. This expression with the fitted value of *C* gave a $\Delta C_p^{\ddagger}$ of 0.73 ± 0.16 kcal mol^{-1} K^{-1} for T_0 = 293.16 K (20 °C). The equilibrium heat capacity change, $\Delta C_{p,U}$, for 434 Cro folding is 1.0 ± 0.10 kcal mol^{-1} K^{-1}

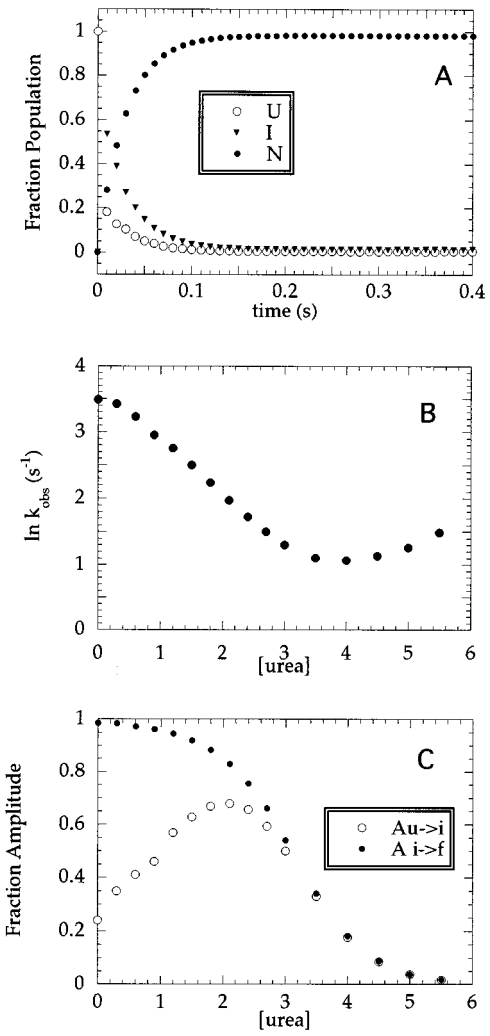

FIGURE 6: Simulated refolding kinetics of 434 Cro at pH 6.0 and 20 °C, assuming an "on-pathway" model. The parameters used in the U ↔ I ↔ ‡ ↔ N simulation were as follows: $\Delta G = 0$ and $m = 0$ for U, $\Delta G = -0.63$ kcal mol^{-1} and $m = 0.70$ kcal mol^{-1} M^{-1} for I, $\Delta G = 15$ kcal mol^{-1} and $m = 0.80$ kcal mol^{-1} M^{-1} for ‡, and $\Delta G = -3.14$ kcal mol^{-1} and $m = 1.00$ kcal mol^{-1} M^{-1} for N. k_{obs} between U and I was set to a high value, e.g., 10 000 s^{-1}, and the rates between I and ‡ and between ‡ and N were calculated using the Eyring equation and the free energy difference of the barrier heights. (A) Populations of U (○), I (▼), and N (●) during the refolding of 434 Cro at 0 M urea. (B) k_{obs} for the disappearance of U (or formation of I) from the simulation. (C) Variation in the amplitudes (A) in the U → I (○) and I → N (●) steps of folding vs [urea]. Note that the observed amplitude for U → I reaches a maximum near 2 M urea as does the experimental refolding amplitude.

(*29*). Therefore, most of the heat capacity change takes place when the unfolded state passes to the transition state.

DISCUSSION

434 Cro Folding Stability and Kinetics. Folding of 434 Cro occurs in the millisecond time range, and it unfolds on the time range of seconds at 20 °C as measured by stopped-flow fluorescence well within the limits defined in manual mixing and NMR experiments. Since the slopes, m_f and m_u, describing the urea dependence of the refolding and unfolding rates are proportional to the change in the amount of surface area buried, these chevron plots also provide information about the nature of the transition state ensemble

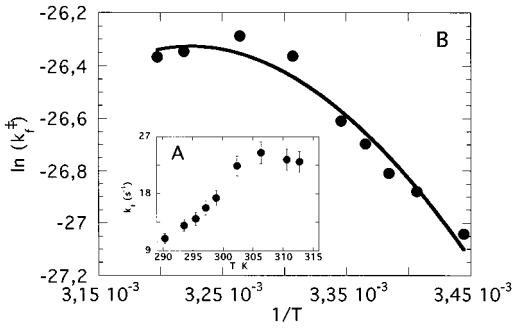

FIGURE 7: Temperature dependence of 434 Cro refolding rates. The final urea concentration was 1.5 M in pH 6.0 buffer. (A) The folding rates, corrected for the contribution of the unfolding rate at higher temperatures, vs temperature. The error bars indicate the ±7% variation observed among the different shots. (B) The data are replotted as ln($k_f^‡$) vs 1/T. The line is the best least-squares fit to eq 6.

of the folding reaction. At pH 4 and 6, the absolute value of m_f is larger than m_u and α values (eq 4) are closer to 0 than to 1. This is evidence that at either pH the transition state, as monitored by the change in Trp fluorescence, is closer to the native state or, in other words, is passed late in the folding reaction. 434 Cro is less stable at pH 4 than at pH 6 according to equilibrium denaturation experiments (*29*; Table 1). The two-state folding rate in 0 M urea is slower at pH 4 than at pH 6, while the unfolding rate is much faster at pH 4 (Table 2), thus accounting for the decreased stability at pH 4.

The measurement of refolding and unfolding kinetics provides a sensitive test for the two-state nature of a folding reaction since intermediates populated transiently during folding but not present at equilibrium may be detected. Moreover, kinetics can usually be measured over a much wider range of denaturant concentrations than equilibrium measurements. This second point is important because folding intermediates, generally unstable, are most likely to be populated at low denaturant concentrations (*22*). 434 Cro folding is a two-state process under equilibrium conditions (*28*, *29*), and NMR measurements of the folding−unfolding interconversions do not suggest the presence of intermediate forms at equilibrium. Kinetic experiments show a rollover accompanied by an amplitude loss in the refolding limb at pH 6 but not detectable at pH 4, indicating deviation from two-state folding at pH 6. This can be explained by a rapid formation at pH 6 of a refolding intermediate, I, an ensemble in which the Trp, like in the native state, is buried. The refolding amplitude also decreases when there is a change in the fluorescence properties of the unfolded states at low urea versus high urea concentrations, as was reported for the CD properties of unfolded, oxidized ribonuclease A (*52*). We have checked this possibility by measuring the urea dependence of the fluorescence of folded as well as of acid-unfolded 434 Cro. On going from 0 to 2 M urea, we observed a 10% decrease in the difference of the folded and unfolded fluorescence (data not shown), which is too small to account for the >90% decrease in amplitude observed in the kinetic experiments over this range of urea concentrations (Figure 5C). We conclude that the transient population of a refolding intermediate is the most plausible explanation for the reduced amplitude at low urea concentrations and pH 6.

The experimental refolding data for 434 Cro at pH 6 can be simulated by assuming an on-pathway intermediate, I,

whose Trp is in a native-like environment, whose buried nonpolar surface area is about 70% of that in N, and which is of low stability. At pH 4, the slight deviation from linearity in the unfolding limb of the chevron plot can be explained to a large part as arising from urea-dependent viscosity effects. We emphasize that the viscosity effect on the folding of 434 Cro is assumed. Curvature in chevron plots without any pronounced amplitude decline has been rationalized in terms of shifts in the position of the transition state ensemble as the denaturant concentration is varied (*23*), and so may also contribute in part to the slight observed downward curvature in the unfolding limb of the chevron plots of 434 Cro at pH 4. At equilibrium, the fluorescence of unfolded urea at pH 4 increases with urea concentration (data not shown), resulting in a smaller difference between the fluorescence of the folded and unfolded protein at high urea concentrations. This is the probable cause of the small decrease in the pH 4 kinetic unfolding amplitudes that is apparent at higher urea concentrations (Figure 5D). The proposed on-pathway folding intermediate is based on the fluorescence of Trp60 in 434 Cro. An independent optical probe such as CD could have provided additional insight into the nature of any folding intermediates (*11*, *25*, *49*), but we have not been able to carry out these experiments by CD. A test based on a pulsed-chase hydrogen exchange experiment has been used to confirm and characterize the presence of an on-pathway intermediate for RNaseA (*53*). This approach with 434 Cro is, however, thwarted by the low protection factors in the native state (*28*) and the apparently short lifetime of I (*38*). Off-pathway intermediates have generally been identified with larger proteins which have disulfide bridges, *cis* prolines, and/or tightly bound ligands (*4*−*11*). None of these features are found in the small 434 Cro, so there is little likelihood of I being off-pathway. The sequential folding mechanism with an on-pathway intermediate provides a simple, physically satisfactory description of our experimental data. While the data may be explained equally well by mutiple folding routes and ensembles, such schemes will necessarily be more complex. The folding intermediate in ubiquitin was similarly rationalized to be on-pathway and was suggested to aid in the search for native interactions (*39*).

Changing the pH from 6 to 4 produces two important changes in 434 Cro's folding kinetics. First, there is an increase in the unfolding rate at pH 4 compared to that at pH 6. This is consistent with the observed lower equilibrium stability of 434 Cro at pH 4 (Table 1; *29*). 434 Cro is a highly basic protein (theoretical pI = 10.5), and the lower stability at pH 4 could reflect the higher overall contribution of unfavorable Coulombic repulsions in the folded protein at this pH (*54*). This can be accounted for structurally in terms of stabilizing electrostatic interaction(s) present at pH 6.0 in the native state but absent at pH 4. This would involve groups that titrate around pH 4 like Glu and Asp whose pK_a values are 4.5 ± 0.1 and 4.1 ± 0.1, respectively, in model unstructured peptides (*54*). Likely candidates for the hypothetical electrostatic interaction(s) in 434 Cro would therefore be Glu6, Glu21, Glu49, and Asp57 (Figure 1) whose solvent-exposed side chains would have pK_a values close to those in model peptides. These can form surface ion pairs with the various solvent-exposed Lys or Arg side chains in 434 Cro (*26*, *29*, *31*). The cold shock protein, CspB, in thermophilic and mesophilic bacteria are very similar in sequence, structure, and folding rates, but the thermophilic version is far more stable and unfolds much more slowly (*22*). Favorable surface electrostatic intractions present in the thermophilic protein but missing or unfavorable in the mesophilic one largely account for the slower unfolding kinetics and higher stability of the thermophilic protein (*22*, *55*, *56*).

The second major change in the folding kinetics at pH 4 is the absence or undetectability of the apparent folding intermediate observed at pH 6 at low urea concentrations. This may be explained if an electrostatic interaction were present early in the folding of 434 Cro and stabilizes the intermediate at pH 6, but is absent at pH 4. In wild-type barnase, there is evidence that the folding intermediate inferred from the deviation from a two-state folding behavior (*19*) is stabilized by the buried Asp93−Arg69 salt bridge that likely forms very early in folding (*57*, *58*). In the barnase Asp93 to Asn mutant, this early interaction cannot form, the intermediate is destabilized and so not observed, and the folding kinetics show an apparent two-state behavior (*58*, *59*). Thus, there appear to be parallels in the kinetic behavior observed for 434 Cro at pH 6 and 4. A likely candidate for this hypothetical early interaction in 434 Cro is the buried salt bridge formed by Glu37 and Arg12 (*26*−*29*). We hypothesize that in the unfolded protein at pH 4 Glu37 would be significantly more protonated than at pH 6, and the Glu37−Arg12 salt bridge is formed less frequently early in folding and so is destabilizing to the intermediate. The pK_a of buried Glu37 in native 434 Cro has not been experimentally determined but is probably lower than the model compound value of 4.5 (see ref *29*). And in contrast to the surface salt bridges, the buried Glu37−Arg12 salt bridge would be expected to be present in folded 434 Cro at pH 4 since the energy penalty for the possible shift in the pK_a of Glu37 to keep it charged (<1 kcal mol^{-1}) is less than the energetic cost that would have to be paid for leaving the charged Arg12 in the desolvated, hydrophobic core of the protein (2−5 kcal mol^{-1}; *54*−*62*). This assumes that no gross alterations in native structure occur with the change in pH from 6 to 4. Using PCR mutagenesis, we attempted to substitute each residue of the buried salt bridge pair in 434 Cro with an uncharged isosteric residue to experimentally examine the role of this salt bridge. Protein expression levels were, however, undetectable, and the mutant proteins could not be purified. This was not unexpected since mutations of buried salt bridge residues can be very destabilizing (*54*−*62*), and wild-type 434 Cro has only modest stability. The faster unfolding and lower stability at pH 4 relative to those at pH 6, the native-like transition state at both pHs, and the refolding intermediate present at pH 6 and low urea concentrations but essentially absent at high urea concentrations at pH 6, and at all urea concentrations at pH 4 are summarized by the free energy profile in Figure 8.

The heat capacity change observed during protein folding arises chiefly from the burial of nonpolar groups with a small contribution from polar group burial. We find that roughly three-quarters of the heat capacity change for 434 Cro occurs when the unfolded chain folds to the transition state. This suggests that the protein core is already mostly structured at the transition state, as was concluded from the kinetic *m* and α values. The extent of structure formed in the transition

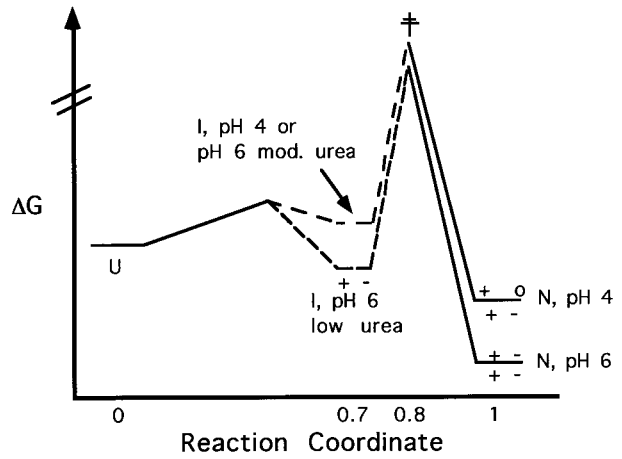

FIGURE 8: Summary scheme of the folding kinetics of 434 Cro. The unfolded ensemble, U, folds via an on-pathway intermediate, I, populated transiently at pH 6 and low urea concentrations, but is too unstable to be populated at pH 4 or at moderate urea concentrations. After passing over the transition state for folding, ‡, the protein reaches the native state, N. The "+ −" symbols above and below the horizontal lines represent surface ion pairs and the buried R12−E37 salt bridge, respectively. The "+ o" symbols at pH 4 indicate the absence of one or more surface ion pairs due to the titration of one or more Glu residues.

state as inferred on the basis of the heat capacity change is somewhat lower than that from the kinetic *m* values, but this discrepancy has also been seen with several other proteins (*17*).

Comparison with λ_{6-85} and Other Systems. 434 Cro is structurally very similar to λ_{6-85} (Figure 1). Table 2 lists kinetic data available for λ_{6-85} for conditions most comparable to those used in this study with 434 Cro. Unfolding rates differ by less than 1 order of magnitude, and the two-state kinetic *m* and α values for the two proteins are similar, indicating native-like transition state for both proteins for the experimental conditions that were used. However, λ_{6-85} and its variant fold in the sub-millisecond time regime and about 2−3 orders of magnitude faster than 434 Cro. Why does 434 Cro fold so much slower than λ_{6-85}? Plaxco et al. (*17*) have shown a correlation between the proximity of the tertiary contacts in a protein, numerically expressed in terms of a contact order, and its folding rate. The contact order for 434 Cro (0.11; K. Plaxco, personal communication) is very close to that of λ_{6-85} (0.094) so that differences in contact order cannot explain the slower folding of 434 Cro.

The rapid folding of λ_{6-85} has, for the most part, been studied by NMR line-shape analysis of exchange-broadened peaks in the presence of moderate concentrations of denaturant required for the presence of sufficient populations of both folded and unfolded forms. This method, as pointed out earlier, measures the folding−unfolding interconversion rates at equilibrium and is unable to detect transient buildups of unstable folding intermediates. For the very rapidly folding variant of λ_{6-85} with two Gly to Ala replacements, stopped-flow fluorescence studies have been reported after engineering in a Trp (*42*), but data at <3.4 M urea or <1.8 M guanidinium hydrochloride could not be obtained because of its extremely fast folding. This could possibly have been less of a problem if such experiments were carried out with wild-type λ_{6-85} into which Trp was engineered to serve as a stopped-flow probe since it folds 1 order of magnitude slower (though still 2 orders of magnitude faster than 434 Cro; Table 2). However, such data are unavailable, to our knowledge. If the rapid folding of λ_{6-85} occurs without any intermediates at low urea concentrations and if the folding intermediate of 434 Cro that we infer in this study is off-pathway and delays its refolding, then this could provide an explanation for why 434 Cro refolds considerably slower than λ_{6-85}. However, the available data do not rule out an intermediate at low urea concentrations for λ_{6-85} (*42*), and for reasons discussed earlier, the 434 Cro folding intermediate is more likely than not to be on-pathway.

434 Cro and λ_{6-85} though structurally homologous are less similar at the level of primary sequence. So their folding need not be governed by the same side chain interactions. In λ_{6-85}, mutations changing local helix stabilities have large effects on folding rates and could be quantitatively linked by means of a diffusion−collision model (*16*, *20*). Increasing intrinsic stabilities of native-like helices by mutation in human procarboxypeptidase A2 (*63*) or the addition of trifluoroethanol, a helix-stabilizing solvent, to human muscle or common-type acylphosphatase (*64*) accelerates folding rates. Thus, the very different folding rates for 434 Cro and λ_{6-85} may be a consequence of different helix propensities. Experimental and/or estimated helix stabilities in 434 Cro and λ_{6-85} indicate that in both proteins helices 1 and 4 are the most stable while the remaining helices have very low or zero propensities (*16*, *31*). Early formation of helices 1 and 4 in λ_{6-85} predicted by the diffusion−collision model mentioned above has been used to explain the fast folding of this protein (*16*). Helices 1 and 4 though intrinsically the most stable ones in 434 Cro are, nevertheless, considerably less so than the corresponding helices in λ_{6-85} (*31*), thereby providing an explanation, at least partly, for the far slower folding rates observed for 434 Cro. The role of intrinsic folding propensities in folding rates is, however, controversial. For instance, the diffusion−collision model linking folding rates and intrinsic helix propensities used with λ_{6-85} (*16*) has also been used to describe the folding of the α-helical GCN-4 coiled coil (*65*), but a differing interpretation has also been put forward (*66*).

Besides differing in helix propensities, another significant difference between 434 Cro and λ_{6-85} is that the buried Arg12−Glu37 salt bridge in 434 Cro discussed earlier does not have a counterpart in λ_{6-85}. A buried salt bridge forms early and is likely to speed the folding of barnase by directing the formation of the hydrophobic core (*58*). On the other hand, in Arc repressor, the presence of unpaired charged groups in the forming hydrophobic core has been elegantly shown to impede folding (*60*). In the case of 434 Cro, direct experimental examination of the role of the buried salt bridge by mutagenesis has not been possible as discussed above, so any conclusions are necessarily speculative. At pH 6 and low urea concentrations, if the buried salt bridge forms more slowly than the hydrophobic core and thereby impedes folding as with the Arc repressor, it could partially account for why 434 Cro folding is slow relative to that of λ_{6-85}. In this hypothesis, the 434 Cro folding intermediate would be off-pathway. As a final point, λ_{6-85} is relatively less basic than 434 Cro (theoretical pI = 7.98 for λ_{6-85} versus 10.5 for 434 Cro), and the resulting differences in electrostatic interactions between the two proteins would also contribute to their distinct stability and folding behavior (*22*, *55*, *56*). Although beyond the scope of the present study, future work

that addresses the nature of these electrostatic contributions would be valuable in adding to our understanding of these effects on protein folding and stability.

For structurally similar proteins, folding mechanisms may or may not be similar (*21*−*25*). Folding pathways are sensitive even to single mutations. In the case of λ_{6-85}, folding is very rapid even as shifts in the transition states and changes in folding mechanisms are affected by mutations or temperature (*20*, *45*). This study has attempted to compare and contrast its folding with that of a structural homologue 434 Cro. Compared to λ_{6-85}, 434 Cro is less stable and folds considerably slower, and the pathway appears to involve a folding intermediate. In vivo, Cro, together with the repressor, controls the switch between lysis and lysogeny in the life cycle of phage 434 by sequence-specific DNA binding (*67*). Remarkably, 434 Cro and the DNA-binding, N-terminal domain of the 434 repressor are almost 50% identical in sequence, and their structures are strikingly similar to one another (and to λ_{6-85}) (*26*−*28*). An examination of the folding kinetics for the 434 repressor N-terminal domain, currently unknown, would add to the growing body of information on the folding of this family of helical proteins and may also provide insight into whether their particular folding behavior has any functional significance. These studies are currently in progress.

ACKNOWLEDGMENT

We thank Dr. S. Subbiah (University of Pennsylvania, Philadelphia, PA) and T. B. Splott for inspiration. We are grateful to the laboratory of Professor S. Harrison (Harvard University, Cambridge, MA) for the gift of plasmids, Professors F. J. Murillo and F. Solano (Universidad de Murcia), Professor G. Giménez-Gallego and Dr. Javier Varela (CIB-Madrid), and Professor F. Blanco (UC-Madrid) for generous access to space and instrumental facilities. We appreciate the calculation of the contact order of 434 Cro by Professor K. W. Plaxco (University of California, Santa Barbara, CA). We thank Dr. J. L. Neira for valuable discussions and Dr. M. Bruix, A. Gómez, and C. López for assistance.

REFERENCES

1. Levinthal, C. (1968) *J. Chem. Phys. 65*, 44−45.
2. Kim, P. S., and Baldwin, R. L. (1990) *Annu. Rev. Biochem. 59*, 631−660.
3. Baldwin, R. L., and Rose, G. D. (1999) *Trends Biochem. Sci. 24*, 77−83.
4. Kiefhaber, T., Grunert, H. P., Hahn, U., and Schmid, F. X. (1992) *Proteins: Struct., Funct., Genet. 12*, 171−179.
5. Weissman, J. S., and Kim, P. S. (1991) *Science 253*, 1386−1393.
6. Darby, N. J., van Mierlo, C. P. M., Scott, G. H. E., Neuhaus, D., and Creighton, T. E. (1992) *J. Mol. Biol. 224*, 904−911.
7. Sosnick, T. R., Mayne, L., Hiller, R., and Englander, S. W. (1994) *Nat. Struct. Biol. 1*, 149−156.
8. Yeh, S.-R., and Rousseau, D. L. (1998) *Nat. Struct. Biol. 5*, 222−228.
9. Kiefhaber, T. (1995) *Proc. Natl. Acad. Sci. U.S.A. 92*, 9029−9033.
10. Rothwarf, D. M., and Scheraga, H. A. (1996) *Biochemistry 35*, 13797−13807.
11. Otzen, D. E., and Oliveberg, M. (1999) *Proc. Natl. Acad. Sci. U.S.A. 96*, 11746−11751.
12. Jackson, S. (1998) *Folding Des. 3*, R81−R91.
13. Dill, K. A., and Chan, H. S. (1996) *Nat. Struct. Biol. 4*, 10−19.
14. Wolynes, P. G., Onuchic, J. N., and Thirumalai, D. (1995) *Science 265*, 1619−1620.
15. Karplus, M., and Weaver, D. L. (1994) *Protein Sci. 3*, 650−668.
16. Burton, R. E., Myers, J. K., and Oas, T. G. (1998) *Biochemistry 37*, 5337−5343.
17. Plaxco, K. W., Simons, K. T., and Baker, D. (1998) *J. Mol. Biol. 277*, 985−994.
18. Matthews, C. R., and Hurle, M. R. (1987) *BioEssays 6*, 254−257.
19. Matouschek, A., Kellis, J. T., Jr., Serrano, L., and Fersht, A. R. (1990) *Nature 346*, 440−445.
20. Burton, R. E., Huang, G. S., Daughtery, M. A., Calderone, T. L., and Oas, T. G. (1997) *Nat. Sruct. Biol. 4*, 305−310.
21. Kragelund, B. B., Hojrup, P., Jensen, M. S., Schjerling, C. K., Juul, E., Knudsen, J., and Poulsen, F. M. (1996) *J. Mol. Biol. 256*, 187−200.
22. Perl, D., Welker, C., Schindler, T., Schröder, K., Marahiel, M. A., Jaenicke, R., and Schmid, F. X. (1998) *Nat. Struct. Biol. 5*, 229−235.
23. Otzen, D. E., Kristensen, O., Proctor, M., and Oliveberg, M. (1999) *Biochemistry 38*, 6499−6511.
24. Martínez, J. C., and Serrano, L. (1999) *Nat. Struct. Biol. 6*, 1010−1016.
25. Dalessio, P. M., and Ropson, I. J. (2000) *Biochemistry 39*, 860−871.
26. Mondragon, A., Wolberger, C., and Harrison, S. C. (1989) *J. Mol. Biol. 205*, 179−188.
27. Mondragon, A., Subbiah, S., Almo, S. C., Drottar, M., and Harrison, S. C. (1989) *J. Mol. Biol. 205*, 189−200.
28. Padmanabhan, S., Jiménez, M. A., González, C., Sanz, J. M., Giménez-Gallego, G., and Rico, M. (1997) *Biochemistry 36*, 6424−6436.
29. Padmanabhan, S., Laurents, D. V., Fernández, A. M., Elías-Arnanz, M., Ruiz-Sanz, J., Mateo, P. L., Rico, M., and Filimonov, V. V. (1999) *Biochemistry 38*, 15536−15547.
30. Huang, G. S., and Oas, T. G. (1995) *Biochemistry 34*, 3884−3892.
31. Padmanabhan, S., Jiménez, M. A., and Rico, M. (1999) *Protein Sci. 8*, 1675−1688.
32. Marqusee, S., and Sauer, R. T. (1994) *Protein Sci. 3*, 2217−2225.
33. Pace, C. N., and Scholtz, J. M. (1996) in *Protein Structure: A Practical Approach* (Creighton, T. E., Ed.) pp 299−321, IRL Press, Oxford, England.
34. Bax, A., and Davis, D. G. (1985) *J. Magn. Reson. 65*, 355−360.
35. Tanford, C. (1970) *Adv. Protein Chem. 24*, 1−95.
36. Eyring, H. (1935) *J. Chem. Phys. 3*, 107−115.
37. Pace, C. N., Laurents, D. V., and Erickson, R. E. (1992) *Biochemistry 31*, 2728−2734.
38. Khorasanizadeh, S., Peters, I. D., Butt, T. R., and Roder, H. (1993) *Biochemistry 32*, 7054−7063.
39. Khorasanizadeh, S., Peters, I. D., and Roder, H. (1993) *Nat. Struct. Biol. 3*, 193−205.
40. Wüthrich, K. (1986) in *NMR of Proteins and Nucleic Acids*, Wiley and Sons Inc., New York.
41. Sato, S., Kuhlman, B., Wu, W.-J., and Raleigh, D. P. (1999) *Biochemistry 38*, 5643−5650.
42. Ghaemmaghami, S., Word, J. M., Burton, R. E., Richardson, J. S., and Oas, T. G. (1998) *Biochemistry 37*, 9179−9185.
43. Schmid, F. X. (1992) in *Protein Folding* (Creighton, T. E., Ed.) pp 197−241, W. H. Freeman, New York.
44. Reimer, U., Scherer, G., Drewello, M., Kruber, S., Schutkowski, M., and Fischer, G. (1998) *J. Mol. Biol. 279*, 449−460.
45. Myers, J. K., and Oas, T. G. (1999) *Biochemistry 38*, 6761−6768.
46. Jacob, M., and Schmid, F. X. (1999) *Biochemistry 38*, 13773−13779.
47. Kawahara, K., and Tanford, C. (1966) *J. Biol. Chem. 241*, 3228−3232.

48. Jonsson, T., Waldburger, C. D., and Sauer, R. T. (1996) *Biochemistry 35*, 4795−4802.
49. Zaidi, F. N., Nath, U., and Udgaonkar, J. B. (1997) *Nat. Struct. Biol. 4*, 1016−1024.
50. Bieri, O., Wildegger, G., Bachmann, A., Wagner, C., and Kiefhaber, T. (1999) *Biochemistry 38*, 12460−12470.
51. Chen, B. L., Baase, W. A., and Schellman, J. A. (1989) *Biochemistry 28*, 691−699.
52. Qi, P. X., Sosnick, T. R., and Englander, S. W. (1998) *Nat. Struct. Biol. 5*, 882−884.
53. Laurents, D. V., Bruix, M., Jamin, M., and Baldwin, R. L. (1998) *J. Mol. Biol. 283*, 669−678.
54. Giletto, A., and Pace, N. C. (1999) *Biochemistry 38*, 13379−13384.
55. Mueller, U., Perl, D., Schmid, F. X., and Heinemann, U. (2000) *J. Mol. Biol. 297*, 975−988.
56. Perl, D., Mueller, U., Heinemann, U., and Schmid, F. X. (2000) *Nat. Struct. Biol. 7*, 380−383.
57. Tissot, A. C., Vuillemier, S., and Fersht, A. (1996) *Biochemistry 35*, 6786−6794.
58. Oliveberg, M., and Fersht, A. (1996) *Biochemistry 35*, 6795−6805.
59. Dao Pin, S., Anderson, D. E., Baase, W., Dahlquist, F. W., and Matthews, B. W. (1991) *Biochemistry 30*, 11521−11529.
60. Waldburger, C. D., Jonsson, T., and Sauer, R. T. (1996) *Nat. Struct. Biol. 2*, 122−128.
61. Waldburger, C. D., Jonsson, T., and Sauer, R. T. (1996) *Proc. Natl. Acad. Sci. U.S.A. 93*, 2629−2634.
62. Pervushin, K., Billeter, M., Siegal, G., and Wüthrich, K. (1996) *J. Mol. Biol. 264*, 1002−1012.
63. Viguera, A. R., and Serrano, L. (1996) *Folding Des. 2*, 23−33.
64. Chiti, F., Taddei, N., Webster, P., Hamada, D., Fiaschi, T., Ramponi, G., and Dobson, C. M. (1999) *Nat. Struct. Biol. 6*, 380−387.
65. Myers, J. K., and Oas, T. G. (1999) *J. Mol. Biol. 289*, 205−209.
66. Moran, L. B., Schneider, J. P., Kentsis, A., Reddy, G. A., and Sosnick, T. R. (1999) *Proc. Natl. Acad. Sci. U.S.A. 96*, 10699−10704.
67. Ptashne, M. (1986) *A Genetic Switch: Gene control and phage λ*, Cell Press and Blackwell Scientific Publications, Cambridge, MA.
68. Kraulis, P. J., Domaille, P. J., Campbell-Burk, S. L., van Aken, T., and Laue, E. D. (1994) *Biochemistry 33*, 3515−3531.

BI001388D